SYNTHESIS OF A SOUND FIELD SCATTERED BY A VIRTUAL OBJECT USING NEAR-FIELD COMPENSATED HIGHER-ORDER AMBISONICS

Nara Hahn and Sascha Spors

Institute of Communications Engineering,
University of Rostock, Germany
{nara.hahn,sascha.spors}@uni-rostock.de

ABSTRACT

For a physically accurate reproduction of a complex virtual sound field, the interaction of sound waves with objects or boundaries have to be taken into account. In this paper, we attempt to synthesize a sound field scattered by an acoustic obstacle. Based on an analytic representation of the incident and scattered sound fields, the loudspeaker driving functions are derived. We explicitly pay attention to the sound obstruction effect behind the scatterer, which is caused by the destructive interference of the incident sound field and the forward scattering. The physical properties of the presented approach are examined through numerical simulations, and the perceptual aspects are discussed in an informal listening test.

1. INTRODUCTION

Sound field synthesis techniques aim at the physical reconstruction of a target sound field within a defined listening area. Typically, a large number of loudspeakers are used, which are termed secondary sources. The secondary sources are driven by individual signals in such a way that the superposition of the reproduced sound fields approximates the desired sound field within the target region. The driving signals are obtained by filtering a source signal with the driving functions, the computation of which depends on the employed sound field synthesis method. Wave Field Synthesis (WFS) [1], near-field compensated higher-order Ambisonics (NFC-HOA) [2], and the spectral division method (SDM) [3] are the best-known analytic methods for sound field synthesis.

The majority of earlier studies on sound field synthesis have focused on the synthesis of virtual sound sources situated in free-field conditions. Real acoustic scenes, however, consist of several objects and boundaries which potentially disturb the sound field. It is known that human auditory perception is influenced by the interaction of sound waves with structures, such as reflection, diffraction, and obstruction [4, 5, 6]. In this study, we are interested in the scattering of an object which causes local variations in the sound field, rather than global modifications due to multiple reflections as in the case of enclosed spaces [7, 8]. In other sound reproduction techniques, scattering and diffraction by a virtual object are often simulated by means of geometrical acoustics, or a digital waveguide model [9, 10, 11]. However, the authors are not aware of similar work in the context of sound field synthesis.

The aim of this paper is to synthesize a sound field scattered by a virtual object, using NFC-HOA (Sec. 2). The analytic driving functions are derived based on the representation of the desired sound field in the spherical harmonics expansion domain (Sec. 3). The presented method is demonstrated by numerical simulation of the synthesized sound field (Sec. 4).

Nomenclature The following notational conventions are used: Vectors are denoted by lowercase boldface $\mathbf{x}$. The spherical coordinate representation of a position vector (r, α, β) is related to the Cartesian coordinate as $x = r\cos\alpha\sin\beta$, $y = r\sin\alpha\sin\beta$, and $z = r\cos\beta$, where r denotes the distance from the origin, α the azimuth angle, and β the colatitude angle. A sound field in the temporal frequency domain is denoted by uppercase $S(\mathbf{x}, \omega)$, where the angular frequency ω is related to the temporal frequency $\omega = 2\pi f$. Monochromatic plane waves are represented with the convention of $e^{-i\langle \mathbf{k}, \mathbf{x}\rangle}$ where the operation $\langle \cdot, \cdot \rangle$ denotes the scalar product, i the imaginary unit, and $\mathbf{k} = (k, \phi_{\text{PW}}, \theta_{\text{PW}})$ the wave vector which indicates the propagation direction. The latter is represented in the Cartesian coordinate as $k_x = k\cos\phi_{\text{PW}}\sin\theta_{\text{PW}}$, $k_y = k\sin\phi_{\text{PW}}\sin\theta_{\text{PW}}$, and $k_z = k\cos\theta_{\text{PW}}$. The norm of $\mathbf{k}$ satisfies the dispersion relation, $\|\mathbf{k}\|^2 = k^2 = \left(\frac{\omega}{c}\right)^2$, with c denoting the speed of sound.

2. NEAR-FIELD COMPENSATED HIGHER-ORDER AMBISONICS

NFC-HOA is based on the explicit solution of the synthesis equation [12, Sec. 1.3]

$$S(\mathbf{x}, \omega) = \int_{\Omega_0} D(\mathbf{x}_0, \omega) G(\mathbf{x} - \mathbf{x}_0, \omega) \mathrm{d}\Omega_0, \tag{1}$$

where $S(\mathbf{x}, \omega)$ denotes the desired sound field, Ω_0 the surface on which the secondary sources are distributed, $D(\mathbf{x}_0, \omega)$ the driving function of the secondary source at $\mathbf{x}_0 = (r_0, \alpha_0, \beta_0) \in \Omega_0$, and $G(\mathbf{x} - \mathbf{x}_0, \omega)$ the spatial transfer function of the corresponding secondary source. NFC-HOA considers only radially symmetric secondary distributions, such as spherical or circular loudspeaker arrays. The synthesis equation is solved with respect to $D(\mathbf{x}_0, \omega)$, by expanding the variables of (1) into the basis solutions of the wave equation, and comparing the expansion coefficients.

2.1. Spherical secondary source distribution

Three-dimensional (3D) NFC-HOA considers spherical distributions of secondary sources. In a spherical configuration, (1) constitutes the surface integral on a sphere with radius r_0, i.e., $\int_{\Omega_0} \mathrm{d}\Omega_0 = \int_0^{2\pi} \int_0^{\pi} r_0^2 \sin\beta_0 \mathrm{d}\beta_0 \mathrm{d}\alpha_0$. The sound field $S(\mathbf{x}, \omega)$ can be expanded into spherical harmonics with respect to the origin [13, Sec. 6.8] as

$$S(\mathbf{x}, \omega) = \sum_{n=0}^{\infty} \sum_{m=-n}^{n} \breve{S}_n^m(\omega) j_n(\tfrac{\omega}{c} r) Y_n^m(\beta, \alpha), \tag{2}$$

where $\breve{S}_n^m(\omega)$ denotes the expansion coefficient, $j_n(\cdot)$ the n-th order spherical Bessel function of the first kind, and $Y_n^m(\beta,\alpha)$ the spherical harmonics. The latter are defined as

$$Y_n^m(\beta,\alpha) = (-1)^m \sqrt{\tfrac{2n+1}{4\pi}\tfrac{(n-|m|)!}{(n+|m|)!}} P_n^{|m|}(\cos\beta) e^{im\alpha}, \quad (3)$$

where $P_n^m(\cdot)$ denotes the m-th order associated Legendre polynomial of degree n. According to the convolution theorem [14, (82)], the spherical harmonics representation of (1) is

$$\breve{S}_n^m(\omega) j_n(\tfrac{\omega}{c}r) = r_0^2 \sqrt{\frac{4\pi}{2n+1}} \breve{D}_n^m(\omega) \breve{G}_n^0(\omega) j_n(\tfrac{\omega}{c}r), \quad (4)$$

where $\breve{G}_n^m(\omega)$ is defined similarly for $G(\mathbf{x}-\mathbf{x}_0,\omega)$ with $\mathbf{x}_0 = (r_0,0,0)$. Thus, the expansion coefficients of the driving function are given as [12, (3.20)]

$$\breve{D}_n^m(\omega) = \frac{1}{r_0^2}\sqrt{\frac{2n+1}{4\pi}} \frac{\breve{S}_n^m(\omega)}{\breve{G}_n^0(\omega)}. \quad (5)$$

The non-uniqueness problem due to the zeros of $j_n(\frac{\omega}{c}r)$ can be overcome and does not affect the solution [15]. Finally, the driving function is given as the spherical harmonics expansion,

$$D_{3\mathrm{D}}(\alpha_0,\beta_0,\omega) = \sum_{n=0}^{\infty}\sum_{m=-n}^{n} \breve{D}_n^m(\omega) Y_n^m(\beta_0,\alpha_0). \quad (6)$$

In case $S(\mathbf{x},\omega)$ is independent of the vertical axis, it can be represented in the circular harmonics domain [13, Sec. 4.3],

$$S(\mathbf{x},\omega) = \sum_{m=-\infty}^{\infty} \mathring{S}_m(\omega) J_m(\tfrac{\omega}{c}r\sin\beta) e^{im\alpha}, \quad (7)$$

where $\mathring{S}_m(\omega)$ denotes the expansion coefficient and $J_m(\cdot)$ the m-th order Bessel function of the first kind. The circular harmonics representation can then be converted to spherical harmonics representation by exploiting [16, Sec. 2.3]

$$\breve{S}_n^m(\omega) = 4\pi i^{m-n} Y_n^m(\tfrac{\pi}{2},0)^* \mathring{S}_m(\omega), \quad (8)$$

where $(\cdot)^*$ denotes the complex conjugate. The expansion coefficients of the driving function thus read

$$\breve{D}_n^m(\omega) = \frac{1}{r_0^2}\sqrt{\frac{2n+1}{4\pi}} \frac{4\pi i^{m-n} Y_n^m(\tfrac{\pi}{2},0)^* \mathring{S}_m(\omega)}{\breve{G}_n^0(\omega)}. \quad (9)$$

2.2. Circular secondary source distribution

In practical systems, circular loudspeaker arrays are frequently used, and only a two-dimensional (2D) target field is considered. Theoretically, the synthesis of a 2D sound field requires a circular distribution of secondary line sources, which cannot be realized reasonably so far. A typical loudspeaker rather exhibits a point-source-like radiation. Thus, secondary point sources are considered also for circular arrays. Such a configuration is referred to as 2.5D synthesis, as 2D target sound fields are synthesized by using 3D secondary point sources. Due to the dimensionality mismatch, perfect reconstruction of the desired sound field is not possible, most noticeably due to amplitude deviations [12, Sec. 3.5.2 and 5.3.4].

We assume that the circular array is placed in the xy-plane ($\beta = \frac{\pi}{2}$) centered at the origin. Then, (1) constitutes a circular convolution, $\int_{\Omega_0} \mathrm{d}\Omega_0 = \int_0^{2\pi} r_0 \mathrm{d}\alpha_0$. The expansion coefficients of the 2.5D NFC-HOA driving function are [12, (3.49)],

$$\mathring{D}_m(\omega) = \frac{1}{2\pi r_0} \frac{\breve{S}_{|m|}^m(\omega)}{\breve{G}_{|m|}^m(\omega)}. \quad (10)$$

Note that $\breve{G}_{|m|}^m(\omega)$ is defined for $G(\mathbf{x}-\mathbf{x}_0,\omega)$ where $\mathbf{x}_0 = (r_0, \frac{\pi}{2}, 0)$. The driving function is given as the inverse circular harmonics transform of (10),

$$D_{2.5\mathrm{D}}(\alpha_0,\omega) = \sum_{m=-\infty}^{\infty} \mathring{D}_m(\omega) e^{im\alpha_0}. \quad (11)$$

Similar to (9), if the desired sound field is 2D and represented with $\mathring{S}_m(\omega)$, the expansion coefficients of the driving function are [16]

$$\mathring{D}_m(\omega) = \frac{1}{2\pi r_0} \frac{4\pi i^{m-|m|} Y_{|m|}^m(\tfrac{\pi}{2},0)^* \mathring{S}_m(\omega)}{\breve{G}_{|m|}^m(\omega)}. \quad (12)$$

2.3. Spatial discretization and modal truncation

In real NFC-HOA systems, only a finite number of loudspeakers can be used, and the driving function (6) or (11) has to be spatially discretized. This results in spectral repetitions in the harmonics domain, and introduces spatial aliasing artifacts in the reproduced sound field. Also, the driving functions can be computed only up to a finite order. The maximum order is commonly, but not necessarily, chosen in such a way that the spectral repetitions do not overlap. Then, the synthesized sound field has an artifact-free region around the center of the array. Note that, even if spectral overlaps are avoided, spatial aliasing does occur, due to the spatial bandwidth of practical loudspeakers. A detailed discussion on this topic can be found in [12, Ch. 4].

3. SOUND FIELDS WITH SCATTERING OBJECTS

In this section, we introduce the analytic description of a sound field scattered by an object. The resulting total sound field is given as the superposition of the incident sound field $S_\mathrm{i}(\mathbf{x},\omega)$ and the scattered sound field $S_\mathrm{s}(\mathbf{x},\omega)$ [17],

$$S(\mathbf{x},\omega) = S_\mathrm{i}(\mathbf{x},\omega) + S_\mathrm{s}(\mathbf{x},\omega). \quad (13)$$

The total sound field must satisfy the boundary condition at the surface of the object. If the acoustic impedance at the surface is infinite, or sufficiently larger than the characteristic impedance of the surrounding medium (Z_0), the normal component of the pressure gradient must be equal to zero. This is called sound-hard or rigid boundary condition. If the acoustic impedance equals zero, or negligibly small compared to Z_0, the sound pressure at the surface vanishes. This is called sound-soft or pressure-release boundary condition. The scattered sound field can be computed in the harmonics domain by applying the boundary condition to the individual harmonics. Analytic solutions are known for simple geometries, such as spherical, cylindrical, and planar boundaries.

3.1. Cylindrical scatterers

In this study, we consider a particular example, where an incident plane wave, $S_\mathrm{i}(\mathbf{x},\omega) = e^{-i\langle \mathbf{k},\mathbf{x}\rangle}$, propagates parallel to the xy-plane ($\theta_{\mathrm{PW}} = \frac{\pi}{2}$) and impinges on an infinitely long cylinder, as

illustrated in Fig. 1. This scenario is considered as a first approximation of the scattering by a human body. The axis of the cylinder is assumed to be parallel to the z axis. The radius of the cylinder is denoted by a, and the position of the cylinder is defined as the intersection of its axis with the xy-plane, denoted by $\mathbf{x}_c = (r_c, \alpha_c, \frac{\pi}{2})$. Due to the two-dimensional properties, we only consider the sound field in the xy-plane, in the following.

The spherical and circular harmonics representations of a plane wave are well known, $\breve{S}^m_{\mathrm{i},n}(\omega) = 4\pi i^{-n} Y^m_n(\frac{\pi}{2}, \phi_{\mathrm{PW}})^*$ and $\mathring{S}_{\mathrm{i},m}(\omega) = i^{-m} e^{-im\phi_{\mathrm{PW}}}$, respectively. The driving function can be computed using either of these, leading to the same result.

To represent the scattered field, we employ a local coordinate system as illustrated in Fig. 1. The scattered field is expanded in circular harmonics with respect to $\mathbf{x}_c$ [17, Sec. 2.3.3],

$$S'_{\mathrm{s}}(\mathbf{x}', \omega) = \sum_{\mu=-\infty}^{\infty} \underbrace{e^{-i\langle \mathbf{k}, \mathbf{x}_c\rangle} i^{-\mu} e^{-i\mu\phi_{\mathrm{PW}}} B_\mu(\tfrac{\omega}{c}a)}_{\mathring{S}'_{\mathrm{s},\mu}(\omega)} \times H^{(2)}_\mu(\tfrac{\omega}{c}r') e^{i\mu\phi'}, \quad r' > a, \tag{14}$$

where $H^{(2)}_\mu(\cdot)$ denotes the μ-th order Hankel function of the second kind. The term $B_\mu(\frac{\omega}{c}a)$ is determined according to the boundary condition on the scatterer as

$$B_\mu(\tfrac{\omega}{c}a) = \begin{cases} -\dfrac{J'_\mu(\frac{\omega}{c}a)}{H^{(2)\prime}_\mu(\frac{\omega}{c}a)} & \text{sound-hard} \\ -\dfrac{J_\mu(\frac{\omega}{c}a)}{H^{(2)}_\mu(\frac{\omega}{c}a)} & \text{sound-soft,} \end{cases} \tag{15}$$

where $J'_m(\cdot)$ and $H^{(2)\prime}_m(\cdot)$ denote the derivatives of the respective functions. Equation (14) is valid only in the exterior region, $r' > a$. Note that the scattered sound field can be interpreted as the sound field emitted by a cylindrical radiator.

By exploiting the translation theorem of the Hankel functions [18, Sec. 8.53], the exterior expansion in (14) can be transformed to an interior expansion, thereby translating the expansion center from $\mathbf{x}_c$ to the origin of the global coordinate system,

$$\begin{aligned} S_{\mathrm{s}}(\mathbf{x}, \omega) &= \sum_{\mu=-\infty}^{\infty} \mathring{S}'_{\mathrm{s},\mu}(\omega) \underbrace{\sum_{m=-\infty}^{\infty} H^{(2)}_{m-\mu}(\tfrac{\omega}{c}r_c) e^{-i(m-\mu)\phi_c} J_m(\tfrac{\omega}{c}r) e^{im\phi}}_{H^{(2)}_\mu(\frac{\omega}{c}r')e^{i\mu\phi'}} \\ &= \sum_{m=-\infty}^{\infty} \underbrace{\sum_{\mu=-\infty}^{\infty} \mathring{S}'_{\mathrm{s},\mu}(\omega) H^{(2)}_{m-\mu}(\tfrac{\omega}{c}r_c) e^{-i(m-\mu)\phi_c}}_{\mathring{S}_{\mathrm{s},m}(\omega)} J_m(\tfrac{\omega}{c}r) e^{im\phi}. \end{aligned} \tag{16}$$

Note that this is valid in the interior region, $r < r_c - a$, indicated by the dashed circle in Fig. 1. When substituting $\mathring{S}'_{\mathrm{s},\mu}(\omega)$ in (16) with the terms in (14) and rearranging it, $\mathring{S}_{\mathrm{s},m}(\omega)$ can be represented in terms of $\mathring{S}_{\mathrm{i},m}(\omega)$,

$$\mathring{S}_{\mathrm{s},m}(\omega) = \mathring{S}_{\mathrm{i},m}(\omega) F_m(\mathbf{x}_c, a, \omega) \tag{17}$$

where

$$F_m(\mathbf{x}_c, a, \omega) = e^{-i\langle \mathbf{k}, \mathbf{x}_c\rangle} \sum_{\mu=-\infty}^{\infty} i^{-(\mu-m)} e^{-i(\mu-m)\phi_{\mathrm{PW}}} \times B_\mu(\tfrac{\omega}{c}a) H^{(2)}_{m-\mu}(\tfrac{\omega}{c}r_c) e^{-i(m-\mu)\phi_c}. \tag{18}$$

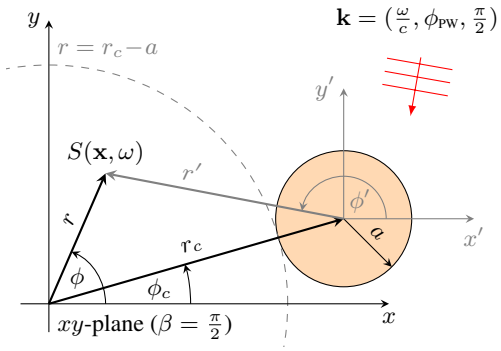

Figure 1: A plane wave propagating parallel to the xy-plane impinges on a cylindrical scatter at $\mathbf{x}_c$. The dashed line indicates the interior region ($r < r_c - a$) of the cylinder.

Therefore, the expansion coefficients of the total sound field are

$$\mathring{S}_m(\omega) = \mathring{S}_{\mathrm{i},m}(\omega)\big(1 + F_m(\mathbf{x}_c, a, \omega)\big). \tag{19}$$

In (18), an infinite summation appears which originally emerges from the exterior expansion in (14). For a given frequency ω, the higher-order terms beyond $\lceil \frac{\omega}{c}a \rceil$ decrease rapidly, and can be neglected in practice. A similar observation for a spherical scatterer can be found in [19, Sec. 4.2].

3.2. NFC-HOA driving functions

We assume that the secondary sources are monopole point sources, and thus, $\breve{G}^m_n(\omega) = -i\frac{\omega}{c} h^{(2)}_n(\frac{\omega}{c}r_0) Y^m_n(\beta_0, \alpha_0)^*$ [13, (8.22)], where $h^{(2)}_n(\cdot)$ indicates the spherical Hankel function of the second kind. The 3D driving function is obtained by plugging (19) into (9),

$$\breve{D}^m_n(\omega) = \frac{1}{r_0^2} \frac{4\pi i^{-n} Y^m_n(\frac{\pi}{2}, \phi_{\mathrm{PW}})^* \big(1 + F_m(\mathbf{x}_c, a, \omega)\big)}{-i\frac{\omega}{c} h^{(2)}_n(\frac{\omega}{c}r_0)}, \tag{20}$$

and the 2.5D driving function is obtained by plugging (19) into (12),

$$\mathring{D}_m(\omega) = \frac{2}{r_0} \frac{i^{-|m|} e^{-im\phi_{\mathrm{PW}}} \big(1 + F_m(\mathbf{x}_c, a, \omega)\big)}{-i\frac{\omega}{c} h^{(2)}_{|m|}(\frac{\omega}{c}r_0)}. \tag{21}$$

4. EVALUATION

The presented approach was implemented in MATLAB using the Sound Field Synthesis toolbox [20]. The driving function for the scattered sound field was additionally implemented in the toolbox for this study. The results for 2.5D NFC-HOA are shown here. A circular loudspeaker array with a radius of $r_0 = 1.5$ m was considered. It consists of $N = 60$ uniformly spaced point sources. The incident plane wave propagates in the negative y-direction, i.e., $\phi_{\mathrm{PW}} = -\frac{\pi}{2}$. A cylindrical scatterer with a radius of $a = 0.4$ m was placed on the y-axis, $\mathbf{x}_c = (2, \frac{\pi}{2}, \frac{\pi}{2})$. Both sound-hard and sound-soft boundary conditions were considered. The driving functions were computed up to a truncated order of 29.

4.1. Monochromatic sound field

The synthesized monochromatic sound fields in the xy-plane are shown in Fig. 2. The secondary sources are indicated by black dots,

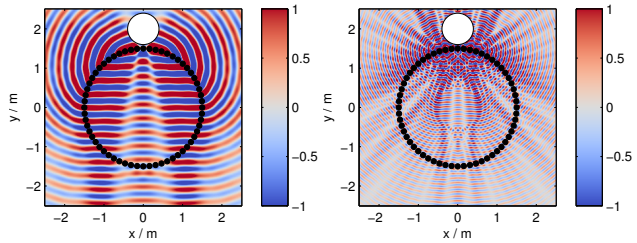

(a) $f = 1$ kHz (b) $f = 3$ kHz

Figure 2: Monochromatic sound field ($N = 60, \phi_{\text{PW}} = -\frac{\pi}{2}, \mathbf{x}_c = (2, \frac{\pi}{2}, \frac{\pi}{2}), a = 0.4$, sound-hard scatterer).

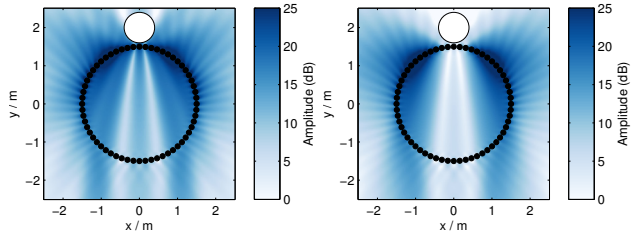

(a) Sound-hard scatterer (b) Sound-soft release

Figure 3: Comparison of amplitude distributions ($N = 60, \phi_{\text{PW}} = -\frac{\pi}{2}, \mathbf{x}_c = (2, \frac{\pi}{2}, \frac{\pi}{2}), a = 0.4, f = 1$ kHz).

and the cylindrical scatterer by a white circle. In Fig. 2a, the spatial structure of the desired sound field is appropriately synthesized within the listening area. As is typically the case in 2.5D synthesis, the synthesized sound field suffers from amplitude errors. Even though, the destructive interference of the incident field and scattered field is properly synthesized. For a higher frequency, shown in Fig. 2b, the desired sound field is correctly synthesized only within a circular region, centered at the origin. This is a well-known property of NFC-HOA [12, Ch. 4], as mentioned in Sec. 2.3.

In Fig. 3, we compared the amplitude distribution of the synthesized sound fields for the same incident plane wave, but with different boundary conditions. The most prominent difference between sound-hard and sound-soft scatterer is observed in the so-called bright zone appearing right behind the cylinder. The bright zone results from the constructive interference of the circumferential waves that propagate along the surface of the cylinder. For sound-soft scatterers, the circumferential waves are more attenuated compared to sound-hard cases, and thus the amplitude in the bright zone is much lower.

4.2. Broadband sound field

To examine the temporal properties, the incident plane wave was driven by a unit impulse in the discrete-time domain. Fig. 4 shows snapshots of the synthesized sound fields at the moment when the incident plane wave passes the origin. In the first case shown in Fig. 4a, the excitation signal is low-pass filtered with a cut-off frequency of 1 kHz which is slightly below the spatial aliasing frequency of the system. The wavefront is deformed in the middle due to diffraction by the scatterer. Figure 4b shows the synthesized sound field for the full-band case. Here, the diffraction and obstruction effects are not clearly visible, due to the additional wavefronts caused by spatial aliasing.

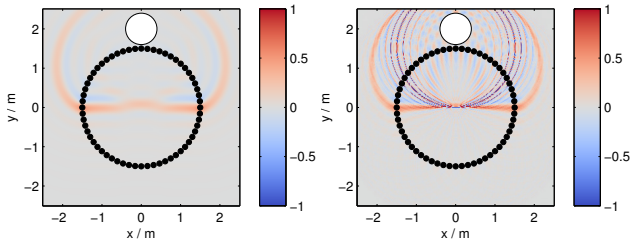

(a) Band-limited (< 1 kHz) (b) Full band

Figure 4: Broadband sound field ($N = 60, \phi_{\text{PW}} = -\frac{\pi}{2}, \mathbf{x}_c = (2, \frac{\pi}{2}, \frac{\pi}{2}), a = 0.4$, sound-hard scatterer).

4.3. Informal listening

For informal listening, the ear signals were simulated for the central listening position. Binaural room impulse responses (BRIRs) were generated by filtering the driving signals with head-related impulse responses [21]. A dynamic scenario was mimicked by concatenating static virtual scenes. A cylindrical scatterer was moved in the positive x-direction along the line $y = 2$ at a constant speed. BRIRs were computed for subsequent scatterer positions on the trajectory with an interval of 5 cm. The ear signals were generated by filtering source signals (speech and castanets) with cross-faded BRIRs. The head orientation was fixed to the positive y direction. The sampling frequency was $f_s = 44.1$ kHz, and c was set to 343 m/s.

As the cylinder approaches the listener from the left, the direct sound arriving on the left ear is first obstructed. The amplitude decrease and spectral change lead to the perception of a sound obstruction. When the cylinder casts a sound shadow on the listener, direct paths are obstructed at both ears. Lower loudness was perceived and the sound was also muffled. However, due to the spatial aliasing artifacts, the high frequency components are less attenuated than one might expect in a real situation. In the case of sound-soft scatterer, the attenuation within the sound shadow is apparently higher than in the sound-hard case, but the spatial aliasing components are still audible causing some unnaturalness.

The listening examples are available for download at `http://spatialaudio.net/nfchoa_virtual_scatterer`. Compare them with the ear signals provided in [22], where the BRIRs were measured in a similar scenario.

5. CONCLUSIONS

In this paper, sound fields interacting with scattering objects were synthesized using NFC-HOA. Based on the analytic representation of the sound field, the 3D and 2.5D driving functions for the scattered field were derived in closed form. Despite the amplitude errors introduced in 2.5D synthesis, the diffraction and sound occlusion of the sound waves were properly synthesized for low frequencies. For high frequencies, however, the spatial aliasing makes the task challenging, as it produces undesired high frequency components to the sound shadow. Virtual sound fields in the presence of a pressure release boundary were also synthesized, which can be rarely experienced in reality. The presented approach is expected to be used for the synthesis of more complex sound fields, where multiple sound sources interact with scattering objects.

6. REFERENCES

[1] A. J. Berkhout, D. de Vries, and P. Vogel, "Acoustic control by Wave Field Synthesis," *J. Acoust. Soc. Am.*, vol. 93, no. 5, pp. 2764–2778, 1993.

[2] J. Daniel, "Spatial sound encoding including near field effect: Introducing distance coding filters and a viable, new Ambisonic format," in *Proc. of 23rd Auido Eng. Soc. Intl. Conference on Signal Processing in Audio Recording and Reproduction*, Helsingør, Denmark, 2003.

[3] J. Ahrens and S. Spors, "Sound field reproduction using planar and linear arrays of loudspeakers," *IEEE Trans. Audio, Speech, and Language Process.*, vol. 18, no. 8, pp. 2038–2050, 2010.

[4] J. Blauert, *Spatial Hearing: The Psychophysics of Human Sound Localization*. MIT press, 1997.

[5] H. Kuttruff, *Room Acoustics*. CRC Press, 2009.

[6] M. S. Gordon and L. D. Rosenblum, "Perception of sound-obstructing surfaces using body-scaled judgments," *Ecol. Psychol.*, vol. 16, no. 2, pp. 87–113, 2004.

[7] D. de Vries, A. J. Reijnen, and M. A. Schonewille, "The wave-field synthesis concept applied to generation of reflections and reverberation," in *Proc. of 96th Audio Eng. Soc. Convention*, Amsterdam, The Netherlands, 1994.

[8] J. Ahrens, "Challenges in the creation of artificial reverberation for sound field synthesis: Early reflections and room modes," in *Proc. of EAA Joint Symp. on Auralization and Ambisonics*, Berlin, Germany, 2014.

[9] M. Vorländer, *Auralization*. Springer, 2007.

[10] D. T. Murphy and M. J. Beeson, "Modelling spatial sound occlusion and diffraction effects using the digital waveguide mesh," in *Proc. of 24th Audio Eng. Soc. Intl. Conference on Multichannel Audio, The New Reality*, Banff, Canada, 2003.

[11] N. Tsingos and J.-D. Gascuel, "Fast rendering of sound occlusion and diffraction effects for virtual acoustic environments," in *Proc. of 104th Audio Eng. Soc. Convention*, Amsterdam, The Netherlands, 1998.

[12] J. Ahrens, *Analytic Methods of Sound Field Synthesis*. Springer, 2012.

[13] E. G. Williams, *Fourier Acoustics: Sound Radiation and Nearfield Acoustical Holography*. Academic press, 1999.

[14] N. Baddour, "Operational and convolution properties of three-dimensional fourier transforms in spherical polar coordinates," *J. Opt. Soc. Am. A.*, vol. 27, no. 10, pp. 2144–2155, 2010.

[15] F. Zotter and S. Spors, "Is sound field control determined at all frequencies? how is it related to numerical acoustics?" in *Proc. of 52nd Audio Eng. Soc. Intl. Conference on Sound Field Control-Engineering and Perception*, Guildford, UK, 2013.

[16] N. Hahn and S. Spors, "Sound field synthesis of virtual cylindrical waves using circular and spherical loudspeaker arrays," in *Proc. of 138th Audio Eng. Soc. Convention*, Warsaw, Poland, 2015.

[17] H. Teutsch, *Modal Array Signal Processing: Principles and Applications of Acoustic Wavefield Decomposition*. Springer Science & Business Media, 2007, vol. 348.

[18] A. Jeffrey and D. Zwillinger, *Table of Integrals, Series, and Products*. Academic Press, 2007.

[19] N. A. Gumerov and R. Duraiswami, *Fast Multipole Methods for the Helmholtz Equation in Three Dimensions*. Elsevier, 2005.

[20] H. Wierstorf and S. Spors, "Sound Field Synthesis toolbox," in *Proc. of 132nd Audio Eng. Soc. Convention*, Budapest, Hungary, 2012.

[21] H. Wierstorf, M. Geier, and S. Spors, "A free database of head related impulse response measurements in the horizontal plane with multiple distances," in *Proc. of 130th Audio Eng. Soc. Convention*, New York, NY, USA, 2011.

[22] N. Hahn and S. Spors, "Measurement of time-variant binaural room impulse responses for data-based synthesis of dynamic auditory scenes," in *Proc. of 40th German Annual Conference on Acoustics (DAGA)*, Oldenburg, Germany, 2014.